Available online at www.sciencedirect.com
ScienceDirect
Trans. Nonferrous Met. Soc. China 31(2021) 2812−2822
Transactions of Nonferrous Metals Society of China
www.tnmsc.cn

Black phosphorous nanosheets−gold nanoparticles−cisplatin for photothermal/photodynamic treatment of oral squamous cell carcinoma

Jun-jie ZENG[1], Zhan-gui TANG[1], Jiao ZOU[2], Jin-gang YU[2]

1. Xiangya Stomatological Hospital, Central South University, Changsha 410006, China;
2. School of Chemistry and Chemical Engineering, Central South University, Changsha 410083, China

Received 15 September 2020; accepted 16 April 2020

Abstract: To improve five-year survival rate of oral squamous cell carcinoma (OSCC), the development of a novel composite material of black phosphorus nanosheets (BPNSs) and gold nanoparticles (AuNPs) for tumor treatment was carried out. The purpose of this study is to evaluate the cytostatic effects of BPNSs, AuNPs loaded with cisplatin (CDDP) on human tongue squamous cell carcinoma cells lines (SCC-9), and 7,12-dimethylbenz anthracene induced cheek squamous cell carcinoma was validated in golden hamsters animal models. The results showed that BPNSs could efficiently inhibit the metastasis and growth of OSCC compared with CDDP and AuNPs. And a combination composite of AuNPs−BPNSs loaded with CDDP could more effectively inhibit the metastasis and growth of OSCC, which might be due to the high drug-loading capacity, excellent photothermal properties and the combination of photodynamic and photothermal therapy of BPNSs and AuNPs, as well as the synergistic effects of AuNPs, BPNSs and CDDP.

Key words: oral squamous cell carcinoma; black phosphorus nanosheets; gold nanoparticles; cancer therapy; tumor biology

1 Introduction

Oral squamous cell carcinoma (OSCC) accounts for more than 90% of all head and neck squamous cell carcinoma cases and is diagnosed as the most common primary tumor in the oral cavity [1]. Currently, the treatment of OSCC has mainly been based on the stage of cancer progression. Early-stage cancers (Stages I and II) can basically be cured by surgery or radiation therapy. However, even with a combination of surgery, radiation and chemotherapy, it is difficult to obtain satisfactory results for the treatment of advanced OSCC (Stages III and IV). Hence, some scholars have studied the chemotherapy regimen to improve the prognosis of patients with OSCC. The use of chemotherapeutic drugs could improve the overall survival rate of patients with oral cancer [2], and the consideration of induction chemotherapy could reduce local recurrence [3]. At present, cisplatin (CDDP) [4], fluorouracil (5-FU) [5], carboplatin [6], paclitaxel [7], methotrexate [8] and so on [9] have been considered to be the most commonly used drugs. Although substantial progresses have been made in cancer chemotherapy, many side effects could be observed due to the unsatisfactory selectivity of chemical agents between normal cells and tumor cells [10]. To overcome the limitations of chemotherapeutic drugs, and realize attenuating and enhancing effects, nanotechnology-based drug treatment has attracted widespread attention. Currently, nanoparticle-based drug loading systems have exhibited higher drug-

Corresponding author: Zhan-gui TANG, Tel: +86-13907317983, E-mail: zhgtang@csu.edu.cn;
Jiao ZOU, Tel/Fax: +86-731-88879616, E-mail: zoujiao@csu.edu.cn
DOI: 10.1016/S1003-6326(21)65695-9

loading capacities and special drug accumulation effects [11].

Various nanoparticles (NPs) and nanosheets (NSs) including magnetic mesoporous silica NPs (MMSNPs) [12], iron oxide NPs [13], graphene oxide NPs (GONPs) [14], gold nanoshells [15], platinum NPs (PtNPs) [16], Ag NPs [17], antimonene NSs (AMNSs) [18], AM quantum dots (AMQDs) [19], Ti_3C_2 NSs [20,21], boron NSs (BNSs) [22], tellurium−selenium (TeSe) NPs [23], black phosphorus NSs (BPNSs) [24−26], and others [27] have been clinically confirmed for the effective treatment of various cancers such as ovarian cancer [28], and oral cancer [29]. Besides, NPs-based drug-loading systems generally possess biocompatible and biodegradable inorganic nanostructures, which could facilitate their use in biomedicine [30,31]. Importantly, some satisfactory results have been obtained by the medical application of NPs in the treatment of OSCC. It is well-known that gold NPs (AuNPs) have been used for the treatment of cancers and human diseases due to their outstanding properties such as reduced cytotoxicity, high stability, easy-to-control sizes and good surface chemistry [32], as well as high surface area/volume ratio and high drug-loading capacity [33]. Meanwhile, AuNPs with strong light absorption can quickly and effectively convert light energy into heat. Therefore, they are usually used as excellent sensitizers for photothermal therapy (PTT) [34]. AuNPs could harvest light in the near-infrared (NIR) region at which the tissue has low absorption and convert it into heat, which could be quickly released in the surrounding tumor tissues [35]. For example, photoactivated AuNPs-mediated PTT has been reported to have grater efficacy in killing breast cancer cells without genetic side effects [36]. With the assistance of a delivery system, a combination of AuNPs with the engineered bi-functional recombinant fusion protein TRAF(C) (TR), the target-specific delivery of an anticancer drug namely doxorubicin (DX) and erbB2-siRNA (si) into ovarian cancer cell lines could be achieved [28]. Compared with traditional drugs, the PTT properties of nanoparticle-based and its drug-loading systems have shown many obvious advantages in terms of drug solubility, number of drug cycles and efficacy [37]. However, concerns have been expressed about the safety and biocompatibility of these nanomaterials.

Recently, newly discovered black phosphorus NPs (BPNSs) have offered some new opportunities for the design of novel electronic and biomedical devices [24]. For example, BPNSs have been considered to be a highly effective photosensitizer and used as a photodynamic treatment (PDT) agent to generate singlet oxygen due to their unique electronic structure and layer-dependent energy band [38]. For instance, PEG-modified BP nanoparticles were used to treat breast tumor by PTT with photoacoustic imaging [39]. In addition, BPNSs could be used as an efficient drug carrier due to their unique puckered lattice configuration and physicochemical properties. Compared with other two dimensional (2D) materials such as grapheme, molybdenum disulfide (MoS_2) and Au nanosheets, BPNSs possess higher drug-loading capacity due to their puckered lattice configuration and higher surface-to-volume ratio [24].

Herein, the effects of BPNSs, AuNPs and CDDP on the growth of OSCC in vitro and in vivo were evaluated. The human SCC-9 cells were employed as in vitro research system, and golden hamster cheek cancer models induced by 7,12-dimethylbenz anthracene (DMBA) were used as in vivo research system. The representative protein index of OSCC was determined by immunohistochemistry. Compared with CDDP, the use of BPNSs or AuNPs had stronger effect on promoting apoptosis of SCC-9 cells. A combination composite of AuNPs and BPNSs loaded with CDDP can effectively inhibit the growth of OSCC, providing some positive evidences for the treatment of OSCC.

2 Experimental

2.1 Chemicals and apparatus

7,12-dimethylbenz anthracene (DMBA) powder was provided by Sigma Chemical Co., BP powder was purchased from Nanjing Ji Cang Nano Technology Co., Ltd. N-methyl-2-pyrrolidone (NMP) was provided by Aladdin Chemistry Co., Ltd. Chloroauric acid tetrahydrated ($HAuCl_4·4H_2O$) was bought from Sinopharm Chemical Reagent Co., Ltd. Trisodium citrate dihyrate (99 wt.%) was obtained from Hunan Huihong Reagent Co., Ltd. Cisplatin (CDDP) was purchased from Shanghai EKEAR Bio@Tech Co., Ltd. Citrate, periodic acid, phosphate-buffered saline (PBS) and diamino-

benzidine were acquired from Sinopharm Chemical Reagent Co., Ltd. Tumor protein p53 (P53) and proliferating cell nuclear antigen (PCNA) were obtained from Wuhan Sanying Biotechnology Co., Ltd. Cell Counting Kit-8 (CCK-8) was provided by Dojindo China Co., Ltd. All reagents were of analytical grade and used without further purification. The aqueous solutions were freshly prepared using double distilled water (DDW). The morphological characterization of BPNSs was carried out on a field emission scanning electron microscopy (FE-SEM, TESCAN MIRA3 LMH/LMU; Czech). The morphologies of BPNSs and AuNPs were characterized using high resolution transmission electron microscopy (HR-TEM, JEM−2100F, JEOL Ltd., Tokyo, Japan). Cytotoxicity and optical density values were analyzed by Microplate Reader (Shenzhen Huisong Technology Development Co., Ltd., Shenzhen, China).

2.2 Preparation of BPNSs and AuNPs

BPNSs were fabricated according to the following procedures: 5.0 mg of BP powder was dispersed in 30.0 mL of NMP solution, and sonicated in an ice-bath for 11 h. After centrifugation at 2000 r/min for 5 min to remove residual unexfoliated particles, the supernatant was collected, then centrifuged at 10000 r/min for 5 min and washed twice with DDW to obtain a brown suspension of BPNSs.

The facile synthesis of AuNPs could be performed by the chemical reduction of $HAuCl_4$ in aqueous solutions [40]. That is, 1.0 mL of 1 wt.% $HAuCl_4$ solution was added immediately to 99.0 mL of DDW which was heated to 60 °C. The mixed solution was heated to boil, and 4.0 mL of trisodium citrate solution was added into the reactor. After 12 min, it was naturally cooled to room temperature to obtain a dispersion of AuNPs.

2.3 Animals and cell cultures

Human tongue squamous cell carcinoma cells line (SCC-9) was purchased from the Cell Bank of the Chinese Academy of Sciences (Shanghai). Golden hamsters were provided by Beijing Vital River Laboratory Animal Technology Co., Ltd., China and were bred in ventilation cages independent of the barrier environment of the Department of Laboratory Animals, Central South University, China.

2.4 Cytotoxicity assay

Cell Counting Kit-8 (CCK-8) analyses were performed to detect the cytotoxicity of BPNSs, AuNPs and CDDP. The cells in the logarithmic growth phase were extracted, digested and counted, and seeded into a 96-well plate at a density of 5×10^4 cells/mL, 100 μL per well. And 5 replicate wells per group were designed. After the cells were adhered, they were treated with different drug-containing media (50 μg/mL of BPNSs dispersion, 50 μg/mL of AuNPs dispersion, 2 mg/mL of CDDP solution, and DDW) for 4 h. After the drug-containing medium was removed, 100 μL of the medium (containing 10 μL of CCK-8) was added to each well. After 4 h of incubation at 37 °C and 5 vol.% CO_2, the optical density (OD) values at 450 nm were analyzed by microplate reader.

2.5 Animal experiments

Healthy golden hamsters were rubbed with 0.5% DMBA in acetone solution on their left cheek pouches three times a week [41]. After 16 weeks, 3 hamsters were randomly executed and their cheek tumor specimens were sent to the Department of Oral Pathology for hematoxylin-eosin staining (HE staining) to identify the nature of the tumor. The remaining mice were divided into 5 groups, which were a combined drug group (the concentration of nanomaterials (BPNSs and AuNPs) was diluted to 50 μg/mL, and the mass ratios (x:y) of AuNPs to BPNSs (AuNPs-to-$BPNSs_{x:y}$) were AuNPs-to-$BPNSs_{5:1}$, AuNPs-to-$BPNSs_{3:1}$, AuNPs-to-$BPNSs_{1:1}$, AuNPs-to-$BPNSs_{1:3}$, AuNPs-to-$BPNSs_{1:5}$, and dissolved in 2 mg/mL of CDDP, respectively), three groups of pure medication group (50 μg/mL BPNSs, 50 μg/mL AuNPs and 2 mg/mL CDDP) and a control group (DDW), respectively. 30 μL of the drug was injected into the remaining golden hamster tumors every three days. After the injection, the tumor was irradiated with infrared rays at a wavelength of 808 nm for 5 min. The survival rates, tumor volumes and mass changes of the golden hamsters during the treatment were recorded. All hamsters were executed 4 weeks after injection of the drug.

2.6 Immunohistochemical assay

At the end of the animal experiment, hamster cheek tumors were collected into paraffin sections

for immunohistochemistry analysis. The sections were incubated at 60 °C for 2 h, immersed in dimethylbenzene to dewax, then dipped in alcohol with a gradually reduced hydrate degree, and washed with DDW. Citrate buffer was used as an antigen retrieval solution to thermally repair sections in a microwave oven. Endogenous peroxidase was inactivated with 1% periodic acid at room temperature. Then, appropriately diluted primary antibodies, PCNA and P53 were added to the sections for incubation, and the sections were stored at 4 °C overnight. The next day, the sections were washed three times with PBS, the secondary antibody was added to incubate for 30 min at 37 °C, and then washed with PBS. The sections were incubated with diaminobenzidine solution as a developer for 5 min at room temperature, followed by DDW washing. Subsequent sections were counterstained with hematoxylin. After rinsing with DDW, the sections were dehydrated with alcohol and cleared with xylene, and then the slides were sealed and observed.

2.7 Statistical analysis

All the data were expressed in the form of mean and error bars (standard deviation of three independent measurements). Kaplan−Meier method was used to analyze survival data. One-way analysis of variance (ANOVA) was performed to assess the significance which was accepted with $p<0.05$. All data analyses were performed using the SPSS 25.0 software.

3 Results and discussion

3.1 Characterization of nanomaterials

BPNSs were coated on an electrode surface for FE-SEM characterization. As shown in Fig. 1(a), BPNSs show discontinuous and nonhomogeneous flake-like structures. The as-prepared BPNSs and AuNPs were characterized by means of HR-TEM. Figures 1(b) and (c) show the HR-TEM images of

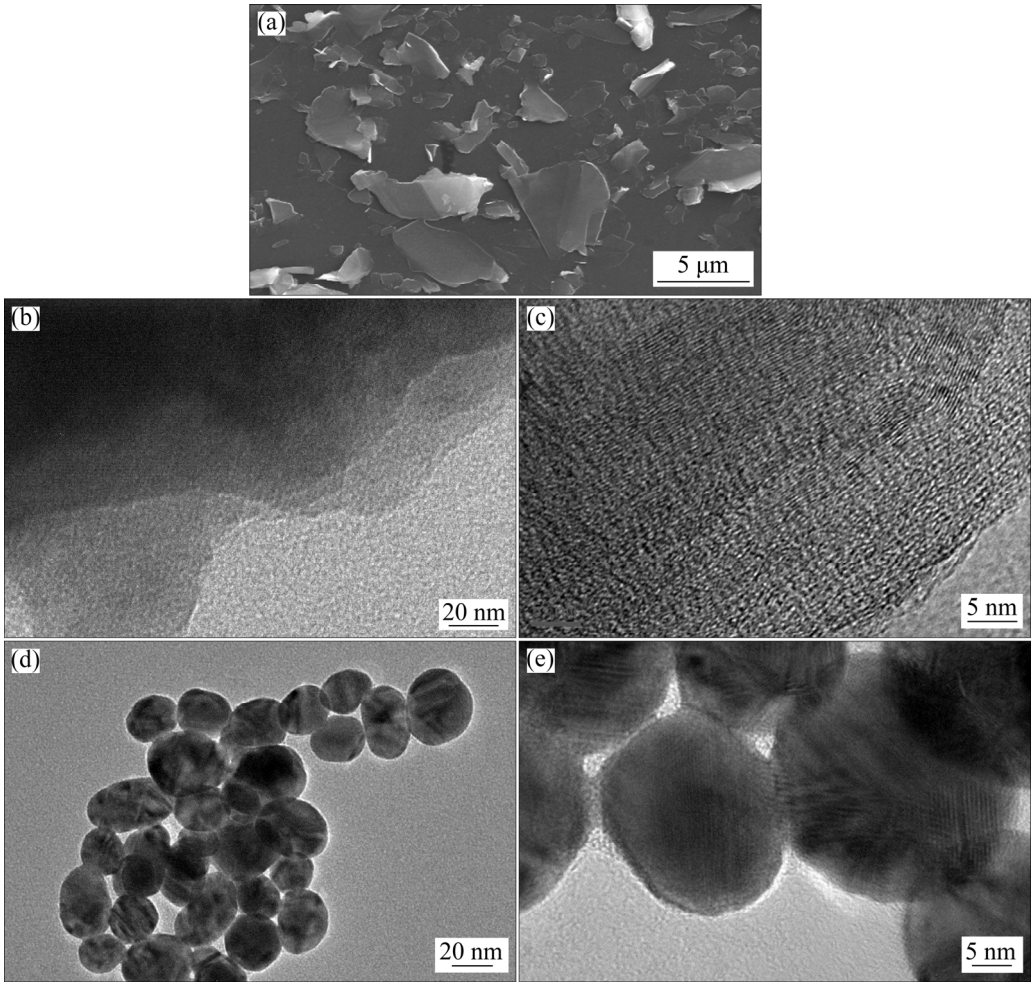

Fig. 1 FE-SEM image of BPNSs on electrode surface (a), and HR-TEM images of nanomaterials of BPNSs (b, c) and AuNPs (d, e)

BPNSs. The typical HR-TEM images indicated that BPNSs having a layered structure with high crystal quality were successfully prepared [42]. As shown in Figs. 1(d, e), AuNPs with an elliptical structure are uniformly dispersed, and the ordered lattices are obvious, indicating that AuNPs possess relatively highly ordered nanostructures and high purity.

3.2 Cytotoxicity of nanomaterials

In the in vitro cytotoxicity experimental, we only used two nanomaterials (BPNSs and AuNPs) to directly treat cells, and the functions of nanomaterials as an efficient drug carrier and photodynamic therapy medium were not compared. The inhibitory effects of BPNSs (50 μg/mL) and AuNPs (50 μg/mL) on human SCC-9 cells were investigated, and DDW was used as a blank control, while the traditional anticancer drug CDDP (2 mg/mL) was used as a positive control. It can be clearly seen form Fig. 2 that the use of low-dose of nanomaterials (BPNSs and AuNPs) can more efficiently promote the apoptosis of human SCC-9 cells compared to the normal doses of CDDP, and BPNSs have shown stronger cells killing ability than AuNPs. AuNPs possessed stronger cells killing ability than CDDP, which might be due to the inhibition of vascular endothelial growth factor 165 to inhibit tumors [43] and the alteration of cell cycle [44]. In addition, BPNSs exhibited the strongest cells killing ability. It might be due to the fact that cancer cells have more vigorous endocytosis and faster metabolic rate than normal cells, BPNSs are easily taken up by cancer cells through endocytosis and rapidly degraded in the cells to produce a large number of phosphate ions. This process led to changes in the internal environment of cancer cells causing G2/M phase arrest, thereby effectively inhibiting the proliferation of cancer cells [10]. After the proliferation was inhibited, cancer cells further entered programmed cells death through apoptosis and autophagy.

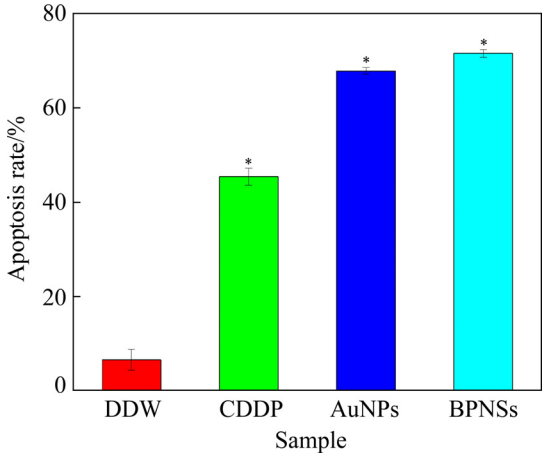

Fig. 2 Effects of BPNSs, AuNPs and CDDP on growth of human SCC-9 cells in cytotoxicity experiments (* Significantly different from DDW group, $p<0.05$)

3.3 Construction of animal model of buccal squamous cell carcinoma

After the potential application of nanomaterials for targeting in vitro was confirmed, we studied the efficacy of nanomaterials in vivo based on established models. As shown in Fig. 3(a), after 16 weeks of DMBA-induced golden hamsters cheek cancer models, the left cheek of the golden hamsters showed tumor-like changes of different sizes. Three golden hamsters were sacrificed, and cheek tumor specimens were collected and sent to HE stained sections to show cancerous tissue. And cancer cells can be seen from HE staining (Fig. 3(b)).

3.4 Inhibition of nanomaterials on golden hamster cheek cancer

Golden hamsters were rubbed with DMBA to induce golden hamster cheek cancer for 16 weeks, and then injected intratumorally for 4 weeks (Fig. 4(a)), and divided into nine groups, namely Group I: untreated (DDW) golden hamsters; Group II: golden hamsters treated with AuNPs-to-$BPNSs_{5:1}$/CDDP complex; Group III: golden hamsters treated with AuNPs-to-$BPNSs_{3:1}$/CDDP complex; Group IV: golden hamsters treated with AuNPs-to-$BPNSs_{1:1}$/CDDP complex; Group V: golden hamsters treated with AuNPs-to-$BPNSs_{1:3}$/CDDP complex; Group VI: golden hamsters treated with AuNPs-to-$BPNSs_{1:5}$/CDDP complex; Group VII: golden hamsters treated with 50 μg/mL BPNSs; Group VIII: golden hamsters treated with 50 μg/mL AuNPs; Group IX: golden hamsters treated with 2 mg/mL CDDP. After the injection, the tumor was irradiated with infrared rays at a wavelength of 808 nm for 5 min.

Since the mortality rate of the golden hamster increased in the last week of the experiment, the data of the first three weeks after injection were selected for comparison. And the survival rates, tumor volumes and mass changes of the golden

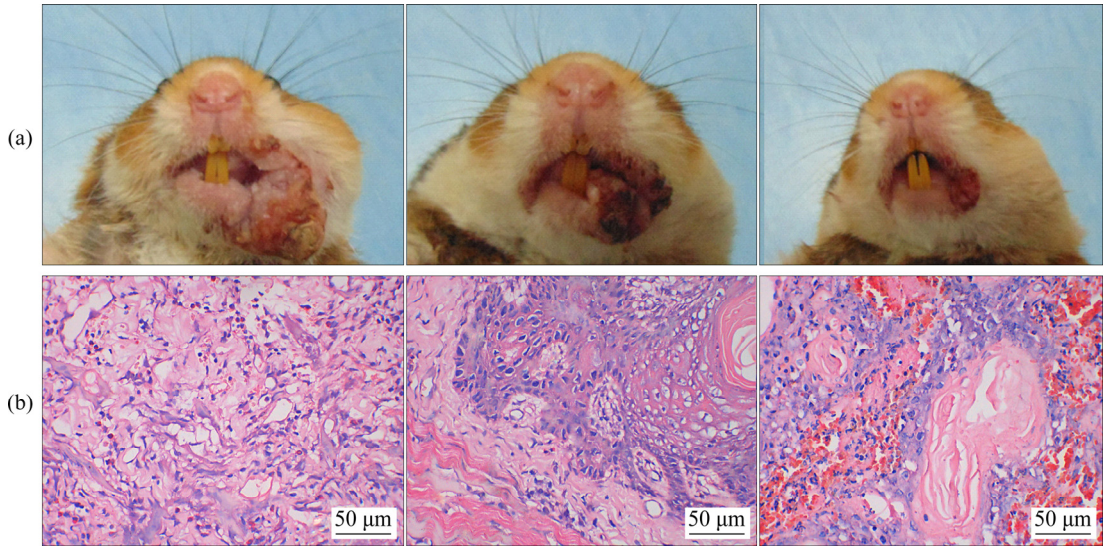

Fig. 3 Models of golden hamster buccal squamous cell carcinoma: (a) Representative images of golden hamster cheek cancer model; (b) Representative images of HE staining

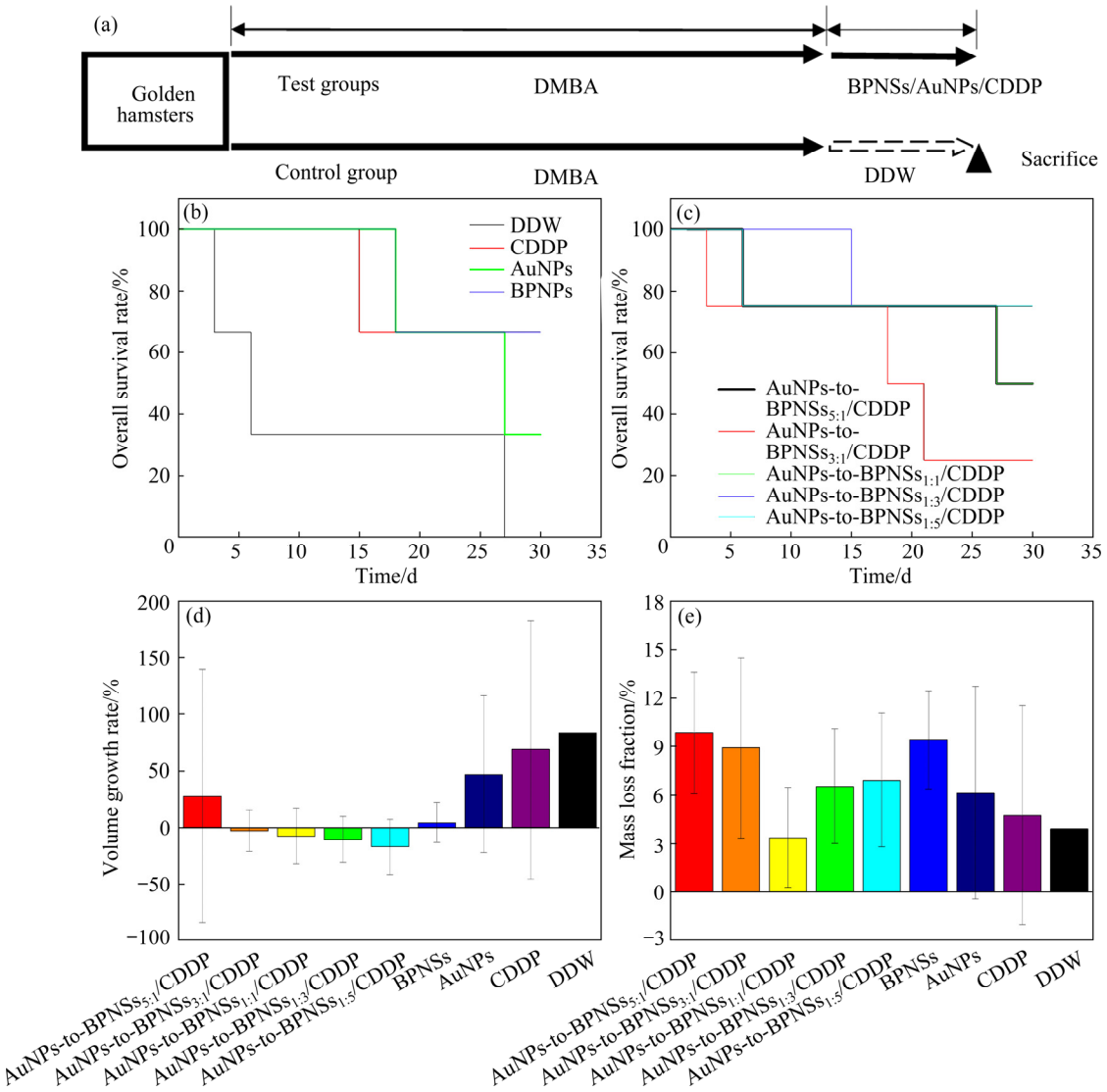

Fig. 4 In vivo models of golden hamsters after injection of drugs (a), survival rate of golden hamsters (b, c), tumor growth and regression (d), and mass change in golden hamsters body (e)

hamsters during the treatment were recorded. As can be seen form Figs. 4(b) and (c), the survival rate of each group of golden hamsters showed that the survival rate of the control group was lower than that of the five groups of combined drug group (AuNPs-to-BPNSs$_{5:1}$/CDDP, AuNPs-to-BPNSs$_{3:1}$/CDDP, AuNPs-to-BPNSs$_{1:1}$/CDDP, AuNPs-to-BPNSs$_{1:3}$/CDDP, and AuNPs-to-BPNSs$_{1:5}$/CDDP) and the three groups of pure medication group (BPNSs, AuNPs and CDDP). The results showed that drug-treated chemotherapy can improve rate of golden hamsters [2]. As can be seen from Fig. 4(b), in the comparison of survival rates among the three pure drug groups, the survival rates of the AuNPs group and the CDDP group were similar, while the survival rate of BPNSs group was significantly higher than both, indicating that BPNSs might benefit from the effect of photothermal therapy, thus has a stronger ability to inhibit cancer cells than AuNPs and CDDP. As shown in Fig. 4(c), among the five groups of combined drug groups, the survival rate of AuNPs-to-BPNSs$_{1:5}$/CDDP was higher than that of AuNPs-to-BPNSs$_{5:1}$/CDDP, further indicating that BPNSs has a stronger ability to inhibit cancer cells than AuNPs.

In addition, the tumor volumes of the golden hamsters were calculated according to the following formula: V=1/2LW^2 (V is the tumor volume, L is the length, and W is the width). It can be clearly seen from Fig. 4(d) that, compared with the control group, all the combined drug groups and the pure drug groups have a certain inhibitory effect on OSCC growth. In particular, the tumor volumes of four combined drug groups (AuNPs-to-BPNSs$_{3:1}$/CDDP, AuNPs-to-BPNSs$_{1:1}$/CDDP, AuNPs-to-BPNSs$_{1:3}$/CDDP and AuNPs-to-BPNSs$_{1:5}$/CDDP) showed negative growth trend, of which the AuNPs-to-BPNSs$_{1:5}$/CDDP had the most obvious antitumor effect, which might be attributed to the drug loading of BPNSs much higher than that of AuNPs [24], and the photothermal effect of BPNSs (808 nm laser irradiated further promotes the release of drugs), as well as synergistic effects of AuNPs, BPNSs and CDDP to enhance the stability and efficacy of nanomaterials drug delivery system.

Furthermore, the mass changes of the golden hamsters during the treatment were recorded. As shown in Fig. 4(e), the mass loss rate of each group of golden hamsters was less than 10%, which might be due to the individual differences of golden hamsters and the space-occupying lesions as well as pain that affects eating, and the toxic and side effects of these drugs were somewhat limited.

3.5 Cytokine response following nanomaterials administration

In order to determine the host immunological response upon treatment with nanomaterials, immunohistochemical experiments were performed on tumor tissues, and the expression of P53 protein and PCNA expression in OSCC tissues were evaluated. P53 protein was thought to counteract oncogenic transformation and tumor growth by preventing the replication of genetically impaired cells [45]. And the expression of PCNA was considered to be positively correlated with the histological grade of OSCC, that is, the increased expression of PCNA might be related to poor tumor differentiation and higher malignancy [46]. As can be seen from Fig. 5(a), in addition to the AuNPs-to-BPNSs$_{1:1}$/CDDP, the expression of a tumor suppressor gene P53 protein in the AuNPs-to-BPNSs$_{5:1}$/CDDP, AuNPs-to-BPNSs$_{3:1}$/CDDP, AuNPs-to-BPNSs$_{1:3}$/CDDP, AuNPs-to-BPNSs$_{1:5}$/CDDP, BPNSs, and AuNPs was higher than that of the CDDP, of which AuNPs-to-BPNSs$_{1:5}$/CDDP exhibited the highest P53 expression, which indicated that AuNPs-to-BPNSs$_{1:5}$/CDDP possessed the strongest inhibitory effect on OSCC due to the fact that the drug loading of BPNSs was much higher than that of AuNPs, and the photothermal therapy effect of BPNSs as well as synergistic effects of AuNPs, BPNSs and CDDP. However, the expression of P53 was the lowest in AuNPs-to-BPNSs$_{1:1}$/CDDP, which may be due to the fact that AuNPs and BPNSs were proportionally equal, and AuNPs were completely attached to the surface of BPNSs, resulting in a decrease in drug loading. As shown in Fig. 5(b), the expression of PCNA by CDDP group was higher than that of other groups, indicating that CDDP alone could not effectively inhibit OSCC, while AuNPs or BPNSs alone had a certain ability to inhibit OSCC. The above histopathological results indicated that the developed nanocomposites (AuNPs-to-BPNSs) loading with CDDP could help to inhibit the growth of OSCC. In particular, the most recently reported results have indicated that BPNSs might carry a risk of developmental perturbation even at lower

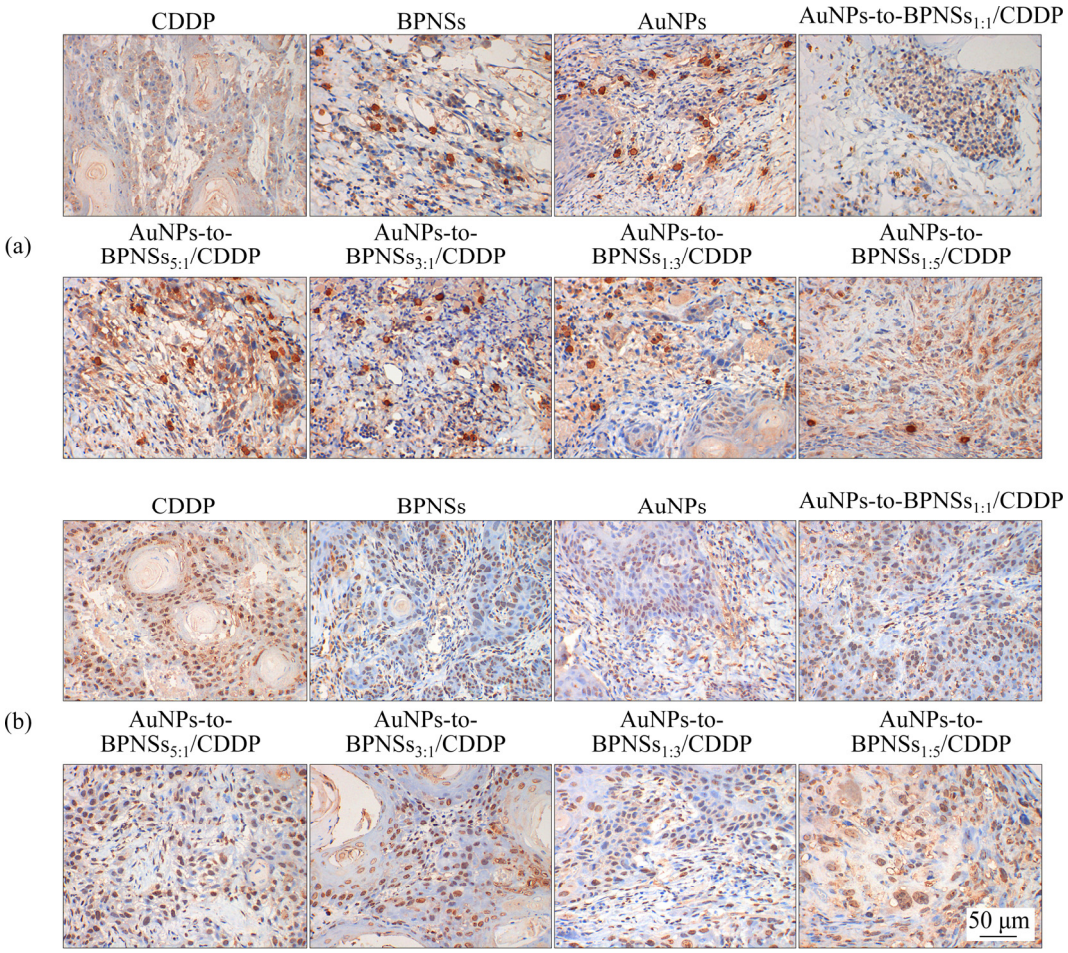

Fig. 5 Immunohistochemical results of tumor tissue (Positive staining is yellow or brownish yellow (dark to brown)): (a) Representative images of P53 protein immunohistochemical staining; (b) Representative images of PCNA immunohistochemical staining

concentrations [47]. Meanwhile, the researches on the toxicity of AuNPs still remain fragmentary and even contradictory with each other due to the variety in experimental conditions [48]. Therefore, more deep researches should be carried out to evaluate their further practical applications.

4 Conclusions

(1) The two nanomaterials (BPNSs and AuNPs) have both shown stronger inhibitory effects on oral squamous cells than the traditional anticancer drug CDDP.

(2) A novel and stable BPNSs- and AuNPs-based drug delivery system (AuNPs-to-BPNSs$_{1:5}$/CDDP) was constructed by the CDDP- loaded AuNPs−BPNSs nanocomposites. The ability of the system to inhibit human SCC-9 cells and buccal squamous cell carcinoma in the golden hamster models was evaluated. The results showed that the tumor suppressor ability of AuNPs-to-BPNSs$_{1:5}$/CDDP was stronger than that of the traditional chemotherapy drug CDDP.

(3) The inhibition of OSCC cells by the system was obvious due to the photothermal effect of BPNSs, which further promoted the release of drug through 808 nm laser magnification. And the high drug loading capacity, excellent photothermal properties and the synergistic effect of photodynamic and photothermal therapy of BPNSs and AuNPs, as well as the synergistic effects of AuNPs, BPNSs and CDDP enhanced the stability and efficacy of nanomaterials drug delivery system.

(4) This approach might provide some new ideas for photothermal therapy based on nanomaterials and a new perspective for the treatment of OSCC.

Acknowledgments

The authors are grateful for financial supports from the National Natural Science Foundation of China (No. 81671003), Hunan Graduate Education Innovation and Professional Ability Improvement Project, China (No. CX20200329), and the Fundamental Research Funds for the Central Universities of Central South University, China (No. 2020zzts056).

References

[1] PENG Qian, WANG Yue-hong, QUAN Hong-zhi, LI Yi-ping, TANG Zhan-gui. Oral verrucous carcinoma: From multifactorial etiology to diverse treatment regimens [J]. International Journal of Oncology, 2016, 49(1): 59−73.

[2] FURNESS S, GLENNY A M, WORTHINGTON H V, PAVITT S, OLIVER R, CLARKSON J E, MACLUSKEY M, CHAN K K W, CONWAY D I. Interventions for the treatment of oral cavity and oropharyngeal cancer: Chemotherapy [J]. Cochrane Database of Systematic Reviews, 2010, 9: CD006386. doi:10.1002/14651858.cd006386.pub2.

[3] LAU A, LI K Y, YANG W F, SU Y X. Induction chemotherapy for squamous cell carcinomas of the oral cavity: A cumulative meta-analysis [J]. Oral Oncology, 2016, 61: 104−114.

[4] HIRAISHI Y, WADA T, NAKATANI K, TOJYO I, MATSUMOTO T, KIGA N, NEGORO K, FUJITA S. EGFR inhibitor enhances cisplatin sensitivity of oral squamous cell carcinoma cell lines [J]. Pathology & Oncology Research, 2008, 14(1): 39−43.

[5] NAKAMURA T, SHINRIKI S, JONO H, UEDA M, NAGATA M, GUO J Y, HAYASHI M, YOSHIDA R, OTA T, OTA K, KAWAHARA K, NAKAGAWA Y, YAMASHITA S, NAKAYAMA H, HIRAKI A, SHINOHARA M, ANDO Y. Osteopontin-integrin alpha(v)beta(3) axis is crucial for 5-fluorouracil resistance in oral squamous cell carcinoma [J]. FEBS Letters, 2015, 589(2): 231−239.

[6] FIDEL J, LYONS J, TRIPP C, HOUSTON R, WHEELER B, RUIZ A. Treatment of oral squamous cell carcinoma with accelerated radiation therapy and concomitant carboplatin in cats [J]. Journal of Veterinary Internal Medicine, 2011, 25(3): 504−510.

[7] JANUS S C, WEURTZ B, ONDREY F G. Inositol hexaphosphate and paclitaxel: Symbiotic treatment of oral cavity squamous cell carcinoma [J]. Laryngoscope, 2007, 117(8): 1381−1388.

[8] DENGRA S, BETHARIA A, BORLE R M, JAJOO S, PATHAK A. Effect of neoadjuvant single drug methotrexate therapy on tumor size reduction in oral squamous cell carcinoma: A pilot study [J]. Indian Journal of Dentistry, 2013, 4(1): 5−11.

[9] MARCAZZAN S, VARONI E M, BLANCO E, LODI G, FERRARI M. Nanomedicine, an emerging therapeutic strategy for oral cancer therapy [J]. Oral Oncology, 2018, 76: 1−7.

[10] ZHOU Wen-hua, PAN Ting, CUI Hao-dong, ZHAO Zhen, CHU P K, YU Xue-feng. Black phosphorus: Bioactive nanomaterials with inherent and selective chemotherapeutic effects [J]. Angewandte Chemie: International Edition, 2019, 131(3): 779−784.

[11] XU Rong, ZHANG Guo-dong, MAI Jun-hua, DENG Xiao-yong, SEGURA-IBARRA V, WU Su-hong, SHEN Jian-liang, LIU Hao-ran, HU Zhen-hua, CHEN Ling-xiao, HUANG Yi, EUGENE K, HUANG Yu, LIU Jun, ENSOR J E, BLANCO E, LIU Xue-wu, FERRARI M, SHEN Hai-fa. An injectable nanoparticle generator enhances delivery of cancer therapeutics [J]. Nature Biotechnology, 2016, 34(4): 414−418.

[12] KNEZEVIC N Z, LIN V S Y. A magnetic mesoporous silica nanoparticle-based drug delivery system for photosensitive cooperative treatment of cancer with a mesopore-capping agent and mesopore-loaded drug [J]. Nanoscale, 2013, 5(4): 1544−1551.

[13] ZHOU Chun-jiao, WANG Shao-hua, ZHOU Yu, RONG Peng-fei, CHEN Zi-zi, LIU Jin-yan, ZHOU Jian-da. Folate-conjugated Fe_3O_4 nanoparticles for in vivo tumor labeling [J]. Transactions of Nonferrous Metals Society of China, 2013, 23(7): 2079−2084.

[14] ZHAO Xu-bo, LIU Lei, LI Xiao-rui, ZENG Jin, JIA Xu, LIU Peng. Biocompatible graphene oxide nanoparticle-based drug delivery platform for tumor microenvironment- responsive triggered release of doxorubicin [J]. Langmuir, 2014, 30(34): 10419−10429.

[15] LIN A W H, LEWINSKI N A, WEST J L, HALAS N J, DREZEK R A. Optically tunable nanoparticle contrast agents for early cancer detection-model-based analysis of gold nanoshells [J]. Journal of Biomedical Optics, 2005, 10(6): 064035.

[16] MANEY V, SINGH M. The synergism of platinum−gold bimetallic nanoconjugates enhances 5-fluorouracil delivery in vitro [J]. Pharmaceutics, 2019, 11(9): 439.

[17] VELGOSOVA O, MRAŽÍKOVÁ A, ČIŽMÁROVÁ E, MÁLEK J. Green synthesis of Ag nanoparticles: Effect of algae life cycle on Ag nanoparticle production and long-term stability [J]. Transactions of Nonferrous Metals Society of China, 2018, 28(5): 974−979.

[18] TAO Wei, JI Xiao-yuan, ZHU Xian-bing, LI Li, WANG Jun-qing, ZHANG Ye, SAW P E, LI Wen-liang, KONG Na, ISLAM M A, GAN Tian, ZENG Xiao-wei, ZHANG Han, MAHMOUDI M, TEARNEY G J, FAROKHZAD O C. Two-dimensional antimonene-based photonic nanomedicine for cancer theranostics [J]. Advanced Materials, 2018, 30(38): 1802061.

[19] TAO Wei, JI Xiao-yuan, XU Xiao-ding, ISLAM M A, LI Zhong-jun, CHEN Si, SAW P E, ZHANG Han, BHARWANI Z, GUO Zi-lei, SHI Jin-jun, FAROKHZAD O C. Antimonene quantum dots: Synthesis and application as near-infrared photothermal agents for effective cancer therapy [J]. Angewandte Chemie: International Edition, 2017, 56(39): 11896−11900.

[20] XING Chen-yang, CHEN Shi-you, LIANG Xin, LIU Quan, QU Meng-meng, ZOU Qing-shuang, LI Ji-hao, TAN Hui, LIU Li-ping, FAN Dian-yuan, ZHANG Han. Two-dimensional MXene (Ti_3C_2)-integrated cellulose hydrogels: Toward smart three-dimensional network nanoplatforms

exhibiting light-induced swelling and bimodal photothermal/chemotherapy anticancer activity [J]. ACS Applied Materials & Interfaces, 2018, 10(33): 27631−27643.

[21] NIE Kai-bo, ZHU Zhi-hao, MUNROE P, DENG Kun-kun, GUO Ya-chao. Microstructure and mechanical properties of TiC nanoparticle-reinforced Mg−Zn−Ca matrix nanocomposites processed by combining multidirectional forging and extrusion [J]. Transactions of Nonferrous Metals Society of China, 2020, 30(9): 2394−2412.

[22] JI Xiao-yuan, KONG Na, WANG Jun-qing, LI Wen-liang, XIAO Yu-ling, GAN S T, ZHANG Ye, LI Yu-jing, SONG Xiang-rong, XIONG Qing-qing, SHI San-jun, LI Zhong-jun, TAO Wei, ZHANG Han, MEI Lin, SHI Jin-jun. A novel top-down synthesis of ultrathin 2D boron nanosheets for multimodal imaging-guided cancer therapy [J]. Advanced Materials, 2018, 30(36): 1803031.

[23] CHEN Shi-you, XING Chen-yang, HUANG Da-zhou, ZHOU Chuan-hong, DING Bo, GUO Zi-heng, PENG Zheng-chun, WANG Dou, ZHU Xi, LIU Shu-zhen, CAI Zhen, WU Jie-yu, ZHAO Jia-qi, WU Zong-ze, ZHANG Yu-hua, WEI Chao-ying, YAN Qiao-ting, WANG Hong-zhong, FAN Dian-yuan, LIU Li-ping, ZHANG Han, CAO Yi-hai. Eradication of tumor growth by delivering novel photothermal selenium-coated tellurium nanoheterojunctions [J]. Science Advances, 2020, 6(15): 6825.

[24] CHEN Wan-song, OUYANG Jiang, LIU Hong, CHEN Min, ZENG Ke, SHENG Jian-ping, LIU Zhen-jun, HAN Ya-jing, WANG Li-qiang, LI Juan, DENG Liu, LIU You-nian, GUO Shao-jun. Black phosphorus nanosheet-based drug delivery system for synergistic photodynamic/photothermal/chemotherapy of cancer [J]. Advanced Materials, 2017, 29(5): 1603864.

[25] WANG Sheng, WENG Jian, FU Xiao, LIN Jing, FAN Wen-pei, LU Nan, QU Jun-le, CHEN Si-ping, WANG Tian-fu, HUANG Peng. Black phosphorus nanosheets for mild hyperthermia-enhanced chemotherapy and chemo-photothermal combination therapy [J]. Nanotheranostics, 2017, 1(2): 208−216.

[26] YANG Xiao-yan, WANG Dong-ya, ZHU Jia-wei, XUE Lei, OU Chang-jin, WANG Wen-jun, LU Min, SONG Xue-jiao, DONG Xiao-chen. Functional black phosphorus nanosheets for mitochondria-targeting photothermal-photodynamic synergistic cancer therapy [J]. Chemical Science, 2019, 10(13): 3779−3785.

[27] ANSELMO A C, MITRAGOTRI S. Nanoparticles in the clinic [J]. Bioengineering & Translational Medicine, 2016, 1(1): 10−29.

[28] KOTCHERLAKOTA R, SRINIVASAN D J, MUKHERJEE S, HAROON M M, DAR G H, VENKATRAMAN U, PATRA C R, GOPAL V. Engineered fusion protein-loaded gold nanocarriers for targeted co-delivery of doxorubicin and erbB2-siRNA in human epidermal growth factor receptor-2^{+} ovarian cancer [J]. Journal of Materials Chemistry B, 2017, 5(34): 7082−7098.

[29] SONG Wen-zhi, GONG Jun-xia, WANG Yu-qian, ZHANG Yan, ZHANG Hong-mei, ZHANG Wei-hang, ZHANG Hu, LIU Xin, ZHANG Tian-fu, YIN Wan-zhong, YANG Wen-sheng. Gold nanoflowers with mesoporous silica as “nanocarriers” for drug release and photothermal therapy in the treatment of oral cancer using near-infrared (NIR) laser light [J]. Journal of Nanoparticle Research, 2016, 18(4): 101.

[30] XIE Zhong-jian, FAN Tao-jian, AN J, CHOI W, DUO Yan-hong, GE Yan-qi, ZHANG Bin, NIE Guo-hui, XIE Ni, ZHENG Ting-ting, CHEN Yun, ZHANG Han, KIM J S. Emerging combination strategies with phototherapy in cancer nanomedicine [J]. Chemical Society Reviews, 2020, 49(22): 8065−8087.

[31] CHEN Jian-ming, FAN Tao-jian, XIE Zhong-jian, ZENG Qi-qiao, XUE Ping, ZHENG Ting-ting, CHEN Yun, LUO Xiao-ling, ZHANG Han. Advances in nanomaterials for photodynamic therapy applications: Status and challenges [J]. Biomaterials, 2020, 237: 119827.

[32] LIAO Jin-feng, QI Ting-ting, CHU Bing-yang, PENG Jin-rong, LUO Feng, QIAN Zhi-yong. Multifunctional nanostructured materials for multimodal cancer imaging and therapy [J]. Journal of Nanoscience and Nanotechnology, 2014, 14(1): 175−189.

[33] CRAIG G E, BROWN S D, LAMPROU D A, GRAHAM D, WHEATE N J. Cisplatin-tethered gold nanoparticles that exhibit enhanced reproducibility, drug loading, and stability: A step closer to pharmaceutical approval? [J]. Inorganic Chemistry, 2012, 51(6): 3490−3497.

[34] ABADEER N S, MURPHY C J. Recent progress in cancer thermal therapy using gold nanoparticles [J]. Journal of Physical Chemistry C, 2016, 120(9): 4691−4716.

[35] KIM H K, HANSON G W, GELLER D A. Are gold clusters in RF fields hot or not? [J]. Science, 2013, 340(6131): 441−442.

[36] GOMAA I E, GABER S A A, BHATT S, LIEHR T, GLEI M, EL-TAYEB T A, ABDEL-KADER M H. In vitro cytotoxicity and genotoxicity studies of gold nanoparticles- mediated photo-thermal therapy versus 5-fluorouracil [J]. Journal of Nanoparticle Research, 2015, 17(2): 102.

[37] LUCKY S S, IDRIS N M, HUANG K, KIM J, LI Z Q, THONG P S, XU R, SOO K C, ZHANG Y. In vivo biocompatibility, biodistribution and therapeutic efficiency of titania coated upconversion nanoparticles for photodynamic therapy of solid oral cancers [J]. Theranostics, 2016, 6(11): 1844−1865.

[38] WANG Hui, YANG Xian-zhu, SHAO Wei, CHEN Shi-chuan, XIE Jun-feng, ZHANG Xiao-dong, WANG Jun, XIE Yi. Ultrathin black phosphorus nanosheets for efficient singlet oxygen generation [J]. Journal of the American Chemical Society, 2015, 137(35): 11376−11382.

[39] SUN Cai-xia, WEN Ling, ZENG Jian-feng, WANG Yong, SUN Qiao, DENG Li-juan, ZHAO Chong-jun, LI Zhen. One-pot solventless preparation of PEGylated black phosphorus nanoparticles for photoacoustic imaging and photothermal therapy of cancer [J]. Biomaterials, 2016, 91: 81−89.

[40] ZHOU Min, WANG Bao-xiang, ROZYNEK Z, XIE Zhao-hui, FOSSUM J O, YU Xiao-feng, RAAEN S. Minute synthesis of extremely stable gold nanoparticles [J]. Nanotechnology, 2009, 20(50): 505606.

[41] KIM S. Animal models of cancer in the head and neck region [J]. Clinical and Experimental Otorhinolaryngology, 2009, 2(2): 55−60.

[42] CHO S Y, LEE Y, KOH H J, JUNG H, KIM J S, YOO H W,

KIM J, JUNG H T. Superior chemical sensing performance of black phosphorus: Comparison with MoS_2 and graphene [J]. Advanced Materials, 2016, 28(32): 7020−7028.

[43] MUKHERJEE P, BHATTACHARYA R, WANG P, WANG L, BASU S, NAGY J A, ATALA A, MUKHOPADHYAY D, SOKER S. Antiangiogenic properties of gold nanoparticles [J]. Clinical Cancer Research, 2005, 11(9): 3530−3534.

[44] ROA W, ZHANG Xiao-jing, GUO Ling-hong, SHAW A, HU Xiu-ying, XIONG Ye-ping, GULAVITA S, PATEL S, SUN Xue-jun, CHEN Jie, MOORE R, XING J Z. Gold nanoparticle sensitize radiotherapy of prostate cancer cells by regulation of the cell cycle [J]. Nanotechnology, 2009, 20(37): 375101.

[45] RENZI A, DE BONIS P, MORANDI L, LENZI J, TINTO D, RIGILLO A, BETTINI G, BELLEI E, SABATTINI S. Prevalence of p53 dysregulations in feline oral squamous cell carcinoma and non-neoplastic oral mucosa [J]. PLoS One, 2019, 14(4): e0215621.

[46] LU E M C, RATNAYAKE J, RICH A M. Assessment of proliferating cell nuclear antigen (PCNA) expression at the invading front of oral squamous cell carcinoma [J]. BMC Oral Health, 2019, 19(1): 233.

[47] YANG Xiao-xi, LIANG Jie-feng, WU Qi, LI Min, SHAN Wan-yu, ZENG Li, YAO Lin-lin, LIANG Yong, WANG Chang, GAO Jie, GUO Ying-ying, LIU Ya-quan, LIU Rui, LUO Qian, ZHOU Qun-fang, QU Guang-bo, JIANG Gui-bin. Developmental toxicity of few-layered black phosphorus toward zebrafish [J]. Environmental Science & Technology, 2021, 55(2): 1134−1144.

[48] JIA Yan-peng, MA Bu-yun, WEI Xia-wei, QIAN Zhi-yong. The in vitro and in vivo toxicity of gold nanoparticles [J]. Chinese Chemical Letters, 2017, 28(4): 691−702.

黑磷纳米片−金纳米颗粒−顺铂光热/光动力治疗口腔鳞癌

曾俊杰[1]，唐瞻贵[1]，邹 娇[2]，于金刚[2]

1. 中南大学 湘雅口腔医院，长沙 410006；
2. 中南大学 化学化工学院，长沙 410083

摘 要：为了改善口腔鳞状细胞癌(OSCC)的较低五年生存率的状况，开发由黑磷纳米片(BPNSs)和纳米金颗粒(AuNPs)组成的复合材料来治疗肿瘤。这项研究的目的是评估 BPNSs、AuNPs 装载顺铂(CDDP)对人舌鳞状细胞癌细胞系(SCC-9)与对 7,12-二甲基苯并蒽诱导的黄金地鼠颊鳞状细胞癌动物模型的抑制作用。结果表明，与 CDDP 和 AuNPs 相比，BPNSs 能更好地抑制 OSCC 的转移和生长。负载 CDDP 的 AuNPs−BPNSs 复合材料可以更有效地抑制 OSCC 的代谢和生长，这可能是归因于 BPNSs 和 AuNPs 的高载药量、优异的光热特性、光动力和光热疗法的结合以及 AuNPs、BPNSs 和 CDDP 的协同作用。

关键词：口腔鳞状细胞癌；黑磷纳米片；纳米金颗粒；癌症治疗；肿瘤生物学

(Edited by Wei-ping CHEN)